Morphing Robots Using Robotic Skins That Sculpt Clay

Dylan S. Shah, Michelle C. Yuen, Liana G. Tilton, Ellen J. Yang, and Rebecca Kramer-Bottiglio

***Abstract*—Shape versatility is a mechanism that many animals leverage to effectively interact-with and locomote-within the natural world. Toward the goal of shape-changing artificial systems, we present morphing robots comprised of robotic skins and sculptable materials. Herein, we describe robotic skins—planar, skin-like substrates with embedded actuation—that are wrapped around sculptable materials in order to actively shape those materials into different forms. Our approach is inspired by the art of sculpture, where surface strains and pressures applied by hand allow clay to be sculpted into nearly any desired shape. Replacing hands with robotic skins, we achieve morphing capabilities in a robotic system. We focus on an example robot in which two robotic skins are layered on a base sculptable material to induce both locomotion and morphing behaviors, and show that morphing enables the robot to overcome obstacles during locomotion. This letter is the first instantiation of morphing robots based on sculpture-inspired surface manipulation of sculptable materials, where shape-changing capabilities are expected to improve robot adaptability to meet the demands of changing environments, overcome obstacles, or perform variable tasks.**

***Index Terms*—Soft material robotics, flexible robots, biologically-inspired robots.**

I. Introduction

SOME biological organisms are able to adjust their body structure and behavior to accommodate a variety of environmental demands and external perturbations. For example, amphibians can regenerate amputated limbs or remodel after structural alteration [1], and metamorphosing creatures such as the tadpole/frog or caterpillar/butterfly can reconfigure their morphology to fit completely different environmental life-styles and operational needs.

Unlike their biological counterparts, current artificial systems (robots) are typically purpose-built for a specific function or finite collection of functions, and have therefore seen limited transition into the natural, unstructured world. The burgeoning use of soft materials in robot constructs (see reviews [2]–[4]) has shown increased resiliency to damage [5], and clever designs have resulted in examples of soft robots that can use their structure to attain multiple locomotion gaits [6], [7]. However, in many cases, robot adaptability requires a change in morphology. Modular and reconfigurable designs have been suggested [7]–[10], although these systems reconfigure via removal and re-addition of parts relative to each other, and are often limited to a discrete range of potential configurations defined by the connections available to the modules. Herein, we introduce a robot that is *self-morphing*, employing robotic skins that transform the morphology of a constant-volume sculptable material using surface actuation.

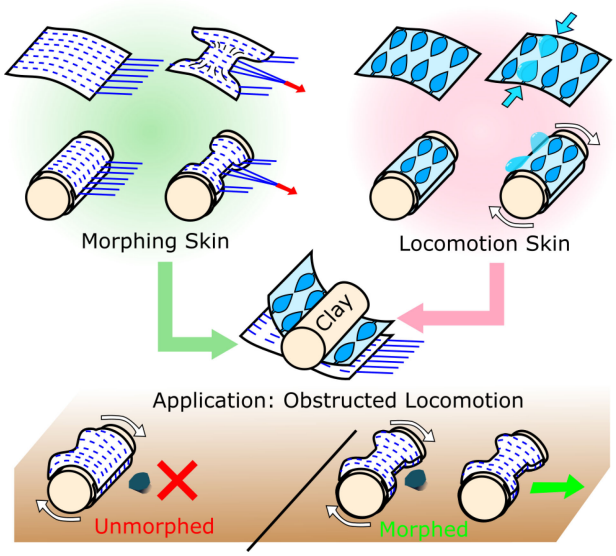

Fig. 1. A morphing robot is created by wrapping robotic skins around a sculptable material. This schematic shows the construction of a robot that changes its shape to overcome an obstacle during locomotion. The example robot comprises two robotic skins: a cable-driven *morphing skin* for shape-changing behavior, and a pneumatic *locomotion skin* for rolling locomotion behavior.

Manuscript received September 10, 2018; accepted January 30, 2019. Date of publication February 27, 2019; date of current version March 11, 2019. This letter was recommended for publication by Associate Editor L. Wen and Editor K.-J. Cho upon evaluation of the reviewers' comments. This work was supported by the National Science Foundation (NSF) under the EFRI program (EFMA-1830870). The work of D. S. Shah was supported by a NASA Space Technology Research Fellowship (80NSSC17K0164). The work of M. C. Yuen was supported by a NSF Graduate Research Fellowship (DGE-1333468). The work of E. J. Yang was supported by a National Aeronautics and Space Administration (NASA) Connecticut Space Consortium Grant (NNX15AI12H). *(Corresponding author: Rebecca Kramer-Bottiglio.)*

D. S. Shah, L. G. Tilton, E. J. Yang, and R. Kramer-Bottiglio are with the Department of Mechanical Engineering and Materials Science, School of Engineering and Applied Science, Yale University, New Haven, CT 06520 USA (e-mail: dylan.shah@yale.edu; ltilton19@students.hopkins.edu; ellen.yang@yale.edu; rebecca.kramer@yale.edu).

M. C. Yuen is with the Department of Mechanical Engineering and Materials Science, School of Engineering and Applied Science, Yale University, New Haven, CT 06520 USA, and also with the School of Mechanical Engineering, Purdue University, West Lafayette, IN 47907 USA (e-mail: michelle.yuen@yale.edu).

This letter has supplementary downloadable material available at http://ieeexplore.ieee.org, provided by the authors. The video shows a morphing robot that uses shape-change to overcome an obstacle during locomotion. For more information, contact rebecca.kramer@yale.edu.

Digital Object Identifier 10.1109/LRA.2019.2902019

We previously introduced the concept of robotic skins that manipulate passive soft bodies [11], which is complementary to the mainstream approach of passive skins with active bodies. Robotic skins are two-dimensional, skin-like, lightweight substrates with embedded actuators, which can be applied-to, removed-from, and transferred-between the surface of any passive soft body to impart motion onto that body. In our prior work, we attached robotic skins to a variety of elastically deformable bodies – such as inert foams, passive tensegrity structures, and human limbs – and generated a wide range of functions – including manipulation, locomotion, and active wearables. In each of these cases, the deformable body produced a restoring force, returning to its original shape after the skin relaxed. Here, we extend the robotic skin concept to moldable, sculptable bodies, treating the robotic skins as surface-based sculptors of the underlying body material to achieve morphing capabilities. Once morphed, the underlying material passively maintains its shape via stress-relaxation, allowing the skin to de-activate and return to a low energy-consumption state.

In this letter, we introduce the concept of morphing robots based on wrapping robotic skins around sculptable material (Fig. 1). To prove the utility and feasibility of this concept, we demonstrate a robot that changes its morphology to overcome an obstacle during locomotion. The example robot comprises two robotic skins layered onto each other and fixed to a sculptable material body. The morphing skin is cable-driven and controls morphing behavior, sculpting the core material into various radially-symmetric shapes such as spheres, cylinders, and dumbbells. The locomotion skin contains thin, pneumatic bladders to produce rolling locomotion when inflated sequentially. We explore several candidate sculptable materials by experimentally characterizing their behavior under compression, and compare these results to *in situ* morphing operations to derive insights on the interplay between the core material behavior and design of the morphing layers and actuation schemes.

II. Materials and Manufacturing

In order to achieve both locomotion and morphing behaviors, we fabricated two robotic skins – one for each behavioral task (which we refer to as the *morphing skin* and the *locomotion skin*). These functional layers can be combined on top of one another, or even integrated by sewing or gluing.

A. Morphing Skin

When a human sculptor shapes clay, force is often exerted downward onto the clay against a tabletop. However, this technique cannot be employed by a lightweight robotic skin since its inertia is not large enough to stabilize itself. Alternatively, circumferential squeezing is attainable since each force has an equal and opposite counterpart, all directed toward the center.

Potential methods of applying a circumferential squeezing force include Pneunets [12] and PneuFlex bending actuators [13] and linearly contracting McKibben actuators [14]. However, we found that these bending actuators require a circumferential restraining layer to push the actuator into the body. McKibben actuators, with their length wrapped around the circumference, have a tendency to flatten the clay rather than squeeze circumferentially. The most promising solution to-date, presented here, uses cables wrapped around a sculptable body to create radially-symmetric forces.

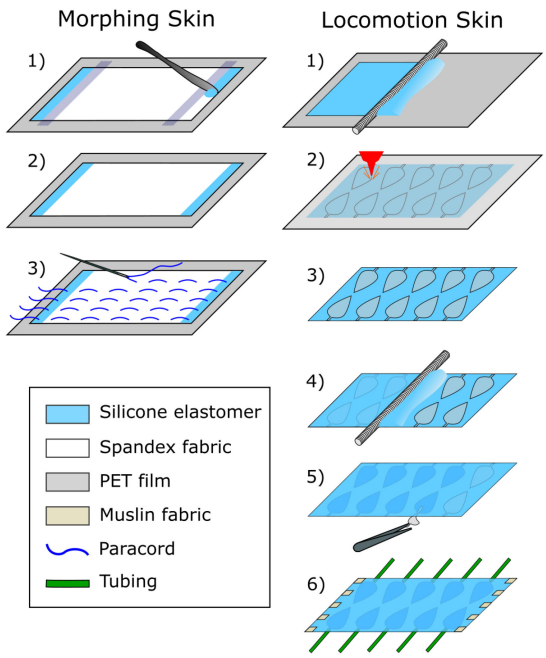

Fig. 2. Fabrication of the cable-driven morphing skin (left) and pneumatic locomotion skin (right).

The morphing skin consists of multiple cables stitched in parallel on a Spandex fabric substrate (Fig. 2, left). First, the shorter edges of the fabric, corresponding to the termini of the cables, were reinforced with silicone elastomer (DragonSkin 10, Smooth-On). Paracord (1.18 mm microcord, Atwood Rope Mfg.) was then stitched into the fabric (15 $\times$ 20 cm) at a stitch spacing of 0.75 cm, and cable-to-cable spacing of 0.75 cm, for a total of 20 cables. 1 cm fabric snaps were attached along the shorter edges of the fabric, in the reinforcement tabs, to allow the skin to be securely wrapped around the clay.

Practical morphing skin design requirements include cable tensile strength, sewability, and appropriate cable spacing. While it may be advantageous to increase cable density to improve the resolution of morphing, as the number of cables increases, issues arising from cable management, cable-on-cable friction, and complexity of associated hardware render the system infeasible. In contrast, sparse cable spacing can result in local pinching and an inability to translate the actuation to global deformation of the clay body. Thus, the design of the morphing skin is driven by compatibility with the material properties of the chosen clay.

During morphing operations, cables of the morphing skin were pulled using a spooling motor (Fig. 3A, B). As shown in Fig. 3B, the cables were fed through sheaths composed of stiff tubing in bundles of five, effectively creating Bowden cables. Five holes were drilled into the tubing, allowing each cable to be fed in with minimal tangling; the holes at the surface of the sheath rested directly against the surface of the morphing skin during contraction. The free ends of the cables were attached

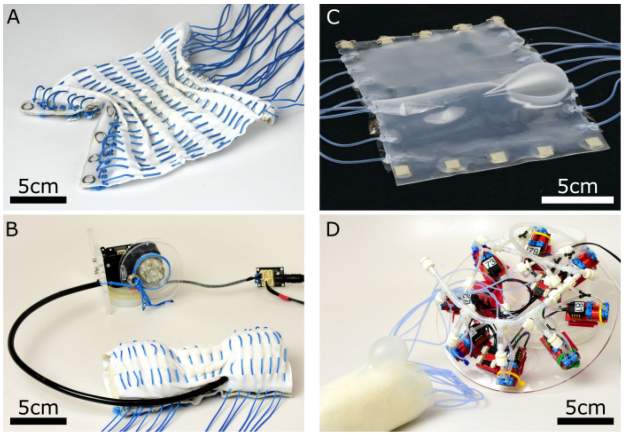

Fig. 3. Photos of the skins and off-board, back-end hardware used to actuate each skin. (A) Photo of the morphing skin. (B) A servomotor spools multiple cables routed through a Bowden cable sheath. (C) Photo of the locomotion skin. (D) A set of 8 pneumatic regulators controls the inflation and deflation of the bladders.

to a spool wound by a servo motor (MX-106R, Dynamixel). During contraction, the free end of the sheath rested directly against the motors' base plates, causing the sheath to undertake the compressive load required to morph the clay.

B. Locomotion Skin

A wide range of robot locomotion strategies exist, including – but not limited to – quadrupedal walking [15], rolling (driven by either controlled shifting of center of mass, or localized extrusion of material) [16], [17], and caterpillar-inspired gaits [7]. Here we exploit rolling locomotion due to its compatibility with a wide range of geometries, enabling the robot to utilize similar gaits across many morphologies.

To achieve locomotion, a series of external-facing, parallel, planar, pneumatic actuators were fabricated in a silicone elastomer film (Fig. 2, right). Silicone elastomer (Dragon Skin 10, Smooth-On) was rod-coated onto PET film to create a $20 \times 15 \times 0.2$ cm layer. After curing, the bladder patterns were lasercut into the PET film, leaving the silicone layer beneath uncut. The portions of the PET film not corresponding to the bladders were peeled away to create a mask for the bladders. Another 0.2 cm thick layer of silicone was then rod-coated over the silicone and PET film masks to form the bladders. Upon curing, excess silicone was trimmed from the edges of the skin, exposing the ends of each of the PET bladders. These pieces of PET were removed by opening up the bladders with reverse tweezers, spraying ethanol into the pocket to release the PET from the silicone, and then pulling out the PET film with tweezers. After allowing the ethanol to evaporate from the bladder, silicone tubing (1/32" ID, McMaster-Carr) was inserted into each bladder and adhered to the skin using silicone elastomer. Small squares of muslin were dipped in silicone and placed on the edges of the skins as attachment points for safety pins that secured the edges of the skin while wrapping it around the clay body.

Various bladder layouts can be fabricated. We considered three layout designs: one, two, and many rows of bladders (a row runs horizontally across the skin as shown in Fig. 2). For the single-row design, the shape of the bladder, as well as defect-free fabrication, is more critical as any asymmetry will result in uneven inflation and thus unintended turning. With the double-row design, asymmetry is less of an issue because each actuator only operates at the ends of the skin. Beyond two rows of bladders, routing the inflation tubes without significant tangling becomes increasingly complex and prohibitive. In this letter, we focus on a design with two columns of parallel teardrop bladders as shown in Fig. 2. The inflation and deflation of each bladder was controlled using digital pneumatic regulators as presented in [18] (Fig. 3C, D).

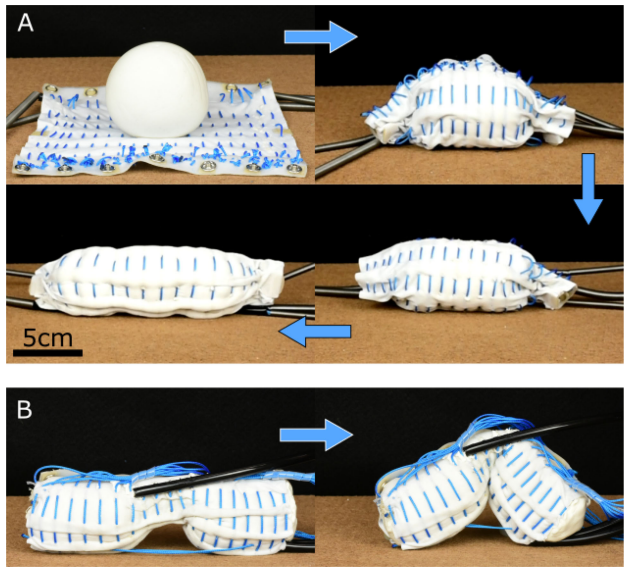

Fig. 4. The morphing skin sculpts clay into different shapes. (A) A sphere of clay is morphed into a cylinder using a morphing skin with cables wrapping around the circumference of the clay. The sphere is morphed into a cylinder by sequentially pulling the cables, starting from the innermost and moving outward. (B) Longitudinally arranged cables are used to morph a dumbbell shape (i.e., a cylinder with an on-demand joint) to an inchworm shape, generating a bending motion about the generated hinge.

III. Robotic Skin Operation

A. Morphing

Morphing behavior was achieved by wrapping the morphing skin around a sculptable body, such as clay. By pulling on a cable, radial contraction of the clay was attained (Fig. 4A). Each cable can change the radius of the circular cross-section it surrounds, so the resulting shapes span all radially-symmetric shapes, such as cylinders, dumbbells, and cones. By positioning cables longitudinally, bending motions can also be attained for shape morphing needs or for inchworm-inspired locomotion (Fig. 4B). While the current work does not demonstrate reversible morphing, preliminary work has suggested that this can be achieved through the addition of inextensible endcaps to the morphing skin, and layering of morphing skins with orthogonal cable directions.

B. Locomotion

When wrapped around the clay body, the locomotion skins operate by sequentially inflating their bladders to continuously

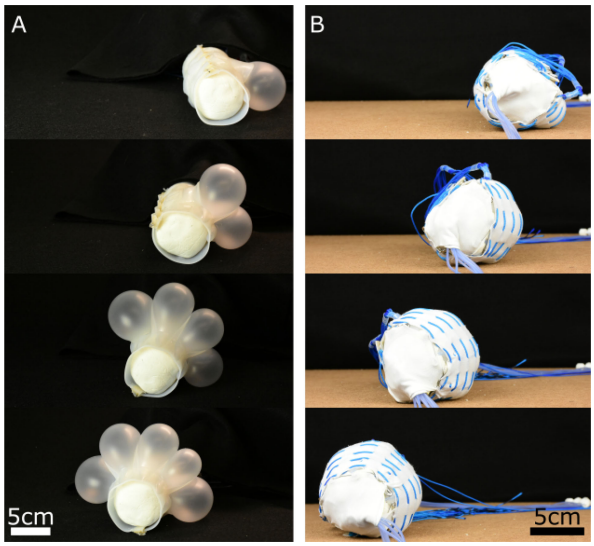

Fig. 5. The locomotion skin operates by inflating the trailing-edge bladder, pushing the robot forward. At an inflation pressure of ≈3 psi, a half rotation takes ≈30 s. (A) Only the locomotion skin is wrapped around clay, showing the bladder expansion. (B) The morphing skin is wrapped over the locomotion skin, showing that rolling can still occur when multiple skins are layered.

tip over, creating a rolling motion (Fig. 5A). Neglecting friction, angular acceleration is proportional to torque (equivalently, tangential force from the bladders) and the mass moment of inertia as $\alpha = T/J$. Therefore, at low accelerations, rolling a chunk of clay can be done with relatively low forces. Here, we found that even small pressures of ≈3 psi were sufficient to inflate the bladders quickly and forcefully enough to be practical in real-time. Higher acceleration could be obtained by integrating fibers perpendicular to the bladders' axes to allow operation at increased pressure, as previously demonstrated by the transition from PneuNets [12] to PneuFlex actuators [13].

C. Combined Morphing and Locomotion

Multiple robotic skins can be layered and fixed onto a sculptable body to achieve their corresponding behaviors in a single system. Here, we layer the morphing skin and the locomotion skin to realize a morphing, locomoting robot. With current hardware, placing the morphing skin underneath the locomotion skin leaves the locomotion skin slack during low-diameter configurations. Thus, to maximize the range of attainable shapes, the morphing skin is used as the outermost layer (Fig. 5B). This arrangement has other benefits: it prevents interaction between the cables and clay, it prevents the clay from drying out, the locomotion skin promotes uniform morphing between cables, and the morphing skin prevents the locomotion skin's bladders from over-inflating. We further note here that during the dozens of tests performed in this study, the skins only failed due to operator error (for example, commanding the robot to over-inflate a silicone bladder).

IV. Designing a Morphing Robot System

When designing a morphing robot system, it is critical to match the forces produced by the morphing skin with the forces required to deform the sculptable body material, among other considerations. Therefore, we sought to identify candidate sculptable materials that: (1) have radial deformation force requirements that can be reasonably produced by a robotic skin; (2) exhibit stress-relaxation, to allow the robot to return to a low-power state after morphing; (3) maintain cohesion over large strains, to allow the robot to undergo significant shape-change without fracturing.

We selected materials by first qualitatively determining the feasibility of several candidate clay-like materials spanning a wide range of material properties: Model Magic modeling compound (Crayola, Pty. Ltd.), Play-Doh modeling compound (Hasbro, Inc.), Protolina No. 1 soft modeling clay (Van Aken International), CoolSand moldable sand (Lisse Inc.), and Sands Alive sand (MCA Sand Co. Ltd.). From this initial assessment, we chose Model Magic for its low stiffness and cohesiveness. We then performed *in situ* tests wherein we deformed a section of a cylindrical billet of Model Magic in a morphing skin using a materials testing machine (Instron 3345) at various compression rates, verifying that commercially available servomotors are suitable for morphing the clay. Seeking a simpler method to characterize potential core materials, we then performed a standard unconfined compression test and an *in situ* test on each candidate material, to determine if and how a simple, standardized unconfined compression test could be used to determine design specifications for the morphing system.

A. Morphing Skin Force Characterization

After initially selecting Model Magic as the "clay," we measured the amount of force required to deform the clay by pulling the cables of the morphing skin wrapped around the clay. For each test, a billet of Model Magic was hand-shaped into a cylinder with initial diameter 6 cm (chosen so the morphing skin was slightly pre-strained when attached) and initial length 15 cm. The morphing skin was wrapped around the cylinder and enclosed in a polycarbonate tube which was secured to the base of the materials testing system. To morph a region of the clay, a bundle of four cables, corresponding to a width w of 2.25 cm, was attached to the load cell and pulled to a 100 mm displacement at five different rates (80, 160, 320, 640, and 1000 mm/min), for five samples each, using the same skin for all tests. This 100 mm change in circumference corresponded to a final diameter of ≈4.4 cm within the squeezed region, and a final diameter of ≈6.2 cm in the region where the cables were not pulled. Note that the diameter predicted by the 100 mm contraction is 2.8 cm. The difference between this prediction and the actual squeezed diameter is primarily due to the clay bulging outward between the cables. Though this inefficiency can be potentially minimized by increasing cable density, manufacturability and cable management would be adversely affected.

At a first estimation, we made some simplifying assumptions: (1) each test can be treated as quasi-static; (2) the clay deformation is radially symmetric; (3) the surface pressure in the squeezed region is homogeneous. Because morphing skins are dynamically modifying their host body, the clay will, in reality, experience non-uniform and time-variant stress. While

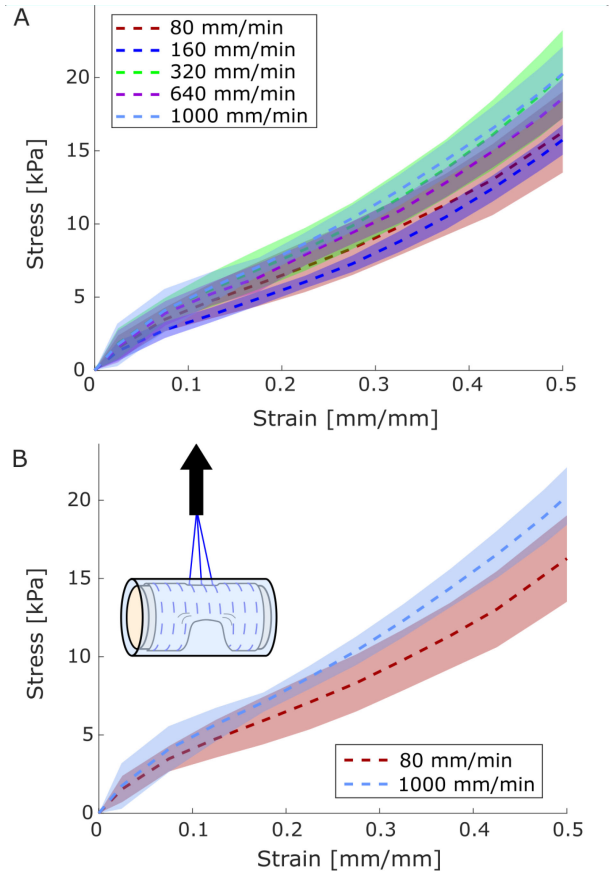

Fig. 6. Plot of the stress vs. strain behavior during *in-situ* radial compression tests. Each curve shows the mean and ±1 standard deviation across five tests. (A) Stress-strain curves for all strain rates, showing significant overlap across all speeds. (B) Stress-strain curves for the lowest and highest strain rates. The schematic shows the experimental setup conceptually.

understanding the magnitude and nature of this stress distribution could potentially lead to increased morphing efficiency, the behavior is material-specific and beyond the scope of this letter. Our assumptions allow us to approximate the normal stress across the outer cylindrical shell as a function of strain in the radial direction from the force vs. extension data measured in the *in situ* morphing skin tests (Fig. 6). In each test, as the cables are pulled to displacement y, the skin presses inward radially so strain ϵ and stress σ are expressed by the following:

$$\epsilon = \frac{r_1 - r_2}{r_1} = \frac{c_1 - c_2}{c_1} = \frac{y}{c_1} \tag{1}$$

$$\sigma = \frac{F}{2\pi r_2 w} = \frac{F}{(2\pi r_1 - y)w} \tag{2}$$

where r_1 and r_2 refer to the initial and instantaneous radii of the squeezed region, c_1 and c_2 refer to the initial and instantaneous circumferences, F is the measured load, and w refers to the width of the cylindrical region being contracted.

The behavior at the various strain rates was similar enough that the confidence intervals overlap significantly (Fig. 6A). For clarity, two representative rates – the slowest and fastest speeds tested – are plotted separately (Fig. 6B). The rate dependence is

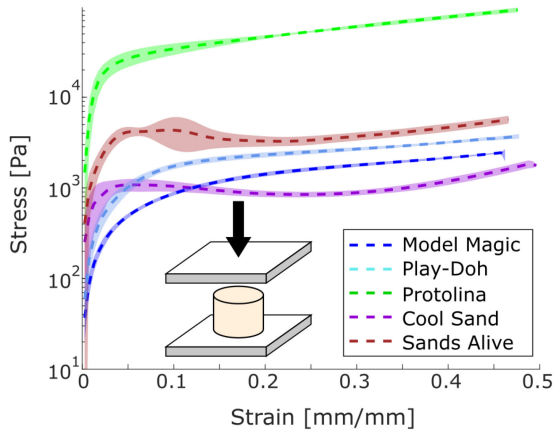

Fig. 7. The stress-strain curves for several candidate materials under an unconfined compression test. Each curve shows the mean and ±1 standard deviation across five tests.

nonzero, but small relative to the overall mechanical response. Therefore, during design of the motor, gearing, and spooling system, there is flexibility in choosing the morphing speed. The force experienced at the full extent of compression was ≈70 N at 80 mm/min, and ≈97 N at 1000 mm/min. With a spool of radius 2 cm attached directly to the motor shaft, 1.4 Nm of torque was required to morph the clay at a rate of 80 mm/min. In comparison, the Dynamixel MX series servomotors utilized here have advertised stall torques ranging from 2.4 to 8.4 Nm.

B. Clay Characterization

After verifying that morphing the clay is possible with the servomotors and is rate-independent over a range of tested speeds (80–1000 mm/min), we then posed the question: "For a given sculptable material, would a simple compression test give enough information to design a compatible morphing skin?" To address this question, we characterized the behavior of all five candidate sculptable materials with an unconfined cylindrical compression test [19], [20]. Each test specimen was shaped in a cylindrical mold with a diameter of 6 cm and height of 6 cm and set in between compression plates mounted to the crosshead and base of the materials testing system (Fig. 7). Fracturing can be seen in the increased standard devaiation of sandy materials, particularly for Sands Alive at ≈15% strain. For water-based materials (Play-Doh, Model Magic), new samples were used during testing to minimize the effect of drying. The material was compressed at a rate of 12.73 mm/min to match the strain experienced in a morphing operation (with cables pulled at at 80 mm/min; $c = 2\pi r$). Since motor torque decreases with angular velocity, a slower morphing rate, such as the one used here, allows for less demanding motor requirements.

To attain the stress vs. strain relationship, we assume that the clay samples maintain constant volume and an approximately cylindrical shape. With an initial geometry of r_1, h_1, and instantaneous geometry of r_2, h_2, we can determine the strain by $\epsilon = \frac{h_1 - h_2}{h_1}$ and the average surface stress in the morphing region σ_{avg} by the measured load F divided by the instantaneous

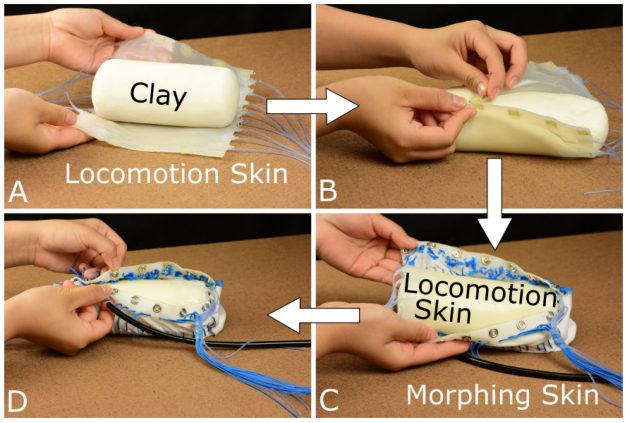

Fig. 8. The clay was first wrapped in the locomotion skin (A-B), followed by the morphing skin (C–D).

contact area, as displacement y is applied:

$$\sigma_{avg} = \frac{F}{\pi r_2^2} = \frac{F}{\frac{\pi r_1^2 h_1}{h_1 - y}} \tag{3}$$

Ideally, the stress-strain curves obtained under this standard test (Fig. 7) should match the stress-strain behavior experienced when using a morphing skin. If so, simple compression tests would enable calculation of the motor torques required to morph the material. However, we found that the stress experienced by the materials during *in situ* tests is significantly higher than in the unconstrained compression test. For Model Magic, the stress at 50% strain during *in situ* tests was $\geq$15 kPa, in comparison to just $\approx$4 kPa during the unconstrained tests. We hypothesize that the discrepancy is mainly due to presence of material neighboring the morphing region, which itself experiences circumferential tension imposed by the morphing skin wrapped around these adjacent sections. Despite these limitations, we found this simple, unconfined compression test to be an efficient tool to quickly compare and evaluate feasibility of candidate materials. For example, the simple compression tests revealed that Protolina (an oil-based technical clay) experiences stresses at least an order of magnitude larger than the other materials, and we therefore removed Protolina from further consideration.

To gain insight into the mechanics of the final multi-skin system, *in situ* morphing tests were performed on the remaining candidate materials by wrapping the material with the locomotion skin followed by the morphing skin, as seen in Fig. 8. In this configuration, the sand-based materials (Sands Alive, CoolSand) had a tendency to exhibit granular jamming at moderate strains ($\approx$15% radial strain), resulting in a sharp increase in stress with added strain. In contrast, the water-based materials (Play-Doh, Model Magic) did not exhibit jamming and required consistently less stress to achieve the same degree of morphing, making them more viable materials for the morphing robot system (Fig. 9). Ultimately, Model Magic was easiest to work with for logistical reasons (did not stick to fabric, and exhibited a slight spring-back effect), and was therefore selected.

We also characterized the materials when wrapped in only the morphing skin (without the underlying locomotion skin). During this characterization, the sand-based materials did not

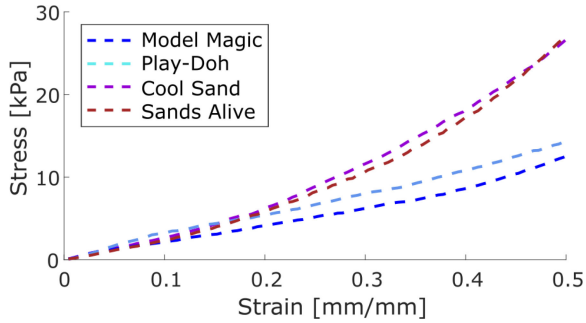

Fig. 9. Stress vs. strain behavior of candidate materials during *in situ* radial compression tests. The material specimens were prepared as in Fig. 8. The cables of the morphing skin were pulled at 80 mm/min as in Fig. 6B. Representative curves for each material are plotted.

exhibit jamming behavior. We hypothesize that the direct contact between cables in the morphing skin and the underlying body material initiating cracking. With the additional locomotion skin base-layer, the material is under uniform external pressure, inducing the jamming effect. Cumulatively, these *in situ* tests highlight the intricate interplay between robotic skins and the materials they are intended to deform or morph.

C. Scalability of Morphing Robots

To design morphing robots at different length scales, changes in motor requirements must also be considered. Consider two morphing robots, robot A and robot B, with the same geometric proportions but at different length scales (initial radii $r_{1A} = Kr_{1B}$, instantaneous radii $r_{2A} = Kr_{2B}$, and morphing region $w_A = Kw_B$, where K is an arbitrary scaling constant). Both morphing robots are driven by the same DC motor at a fixed voltage and the same sized cable spool r_{spool} (i.e., same torque output T_{motor} and applied force $F_{motor} = T_{motor}/r_{spool}$). While morphing at the same cable spooling rate $\dot{y}$, the average surface stress in the morphed region is:

$$\sigma_A = \frac{F_{motor}}{\pi r_{2A} w_A} = \frac{F_{motor}}{\pi K r_{2B} K w_B} = \frac{1}{K^2}\sigma_B \tag{4}$$

Thus, robot B is able to impart $1/K^2$ times as much surface stress onto the clay as robot A. If the morphing speed changes such that the strain rate is held constant, the torque-speed availability of the motors must be considered. Assuming an ideal DC motor which has an affine torque-speed curve connecting stall torque T_s and no-load angular velocity Ω_{NL}, as the cable pull rate increases ($\dot{y_A} = K\dot{y_B}$), the available torques, and corresponding surface forces, decrease as:

$$T_A = \left(\frac{1 - K\Omega_B/\Omega_{NL}}{1 - \Omega_B/\Omega_{NL}}\right) T_B \tag{5}$$

Therefore, with fixed motor and spool parameters, higher surface stress (and range of morphing strains) can be attained by scaling down the robot dimensions. However, scaling down introduces challenges in routing cables from the skin to the motors.

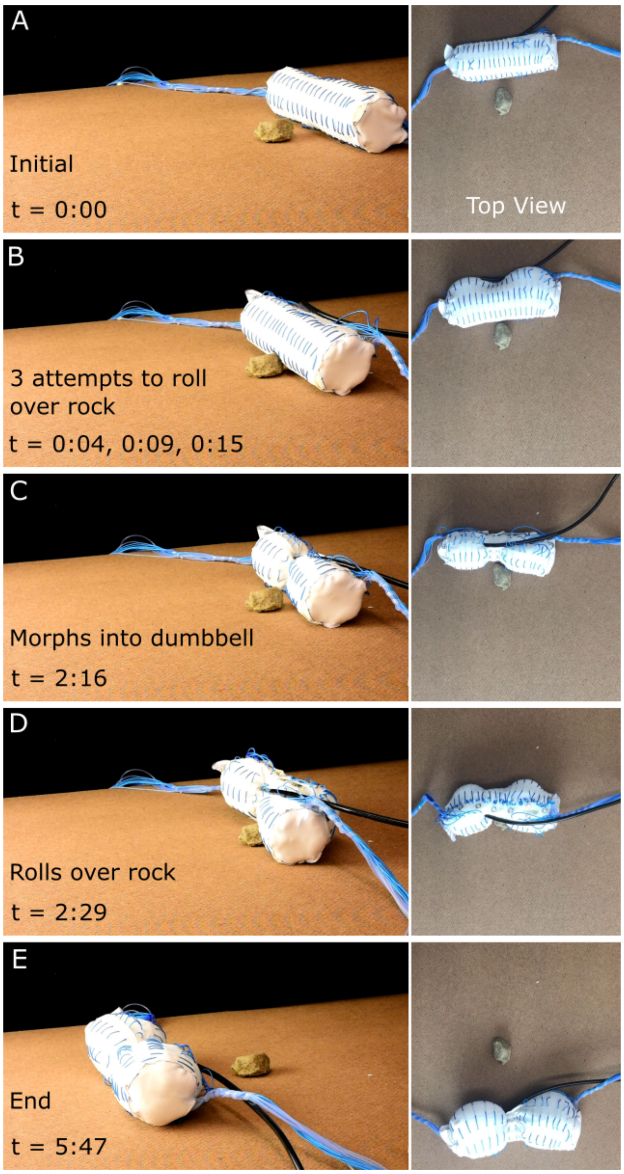

Fig. 10. Layering the morphing skin over the locomotion skin allows the robot to morph to complete tasks such as rolling over an obstacle.

V. Applications

By wrapping both the locomotion and morphing skins around a cylinder of clay (Fig. 8), both locomotion and shape-changing behaviors were achieved. The utility of this approach was demonstrated via an example where the locomoting, morphing robot encountered an obstacle in its path (Fig. 10). First, the initially cylindrical robot rolled on a flat surface (Fig. 10A). Upon encountering an obstacle and failing to roll over it (Fig. 10B), the cylinder was morphed into a dumbbell shape, which allowed the robot to straddle the obstacle (Fig. 10C). Forward locomotion then proceeded, unencumbered by the obstacle (Fig. 10D, E).

Applications where morphing and locomotion might serve as complementary functions are abundant. For the example skins presented in this work, a search-and-rescue operation could use the clay as a medium to hold a payload such as sensors or transmitters. With the ability to morph clay, it would be possible to traverse flat terrain quickly with a large-diameter cylinder. Upon encountering more constrained pathways, the clay could be morphed into a small profile. Here, we showed the robot in a morphed dumbbell shape that enables it to straddle an obstacle and continue rolling. Throughout these contortions, the sensors and transmitter payload would remain held in the clay body. More broadly, applications include resource-limited conditions where supply chains for materiel are sparse. For example, the morphing sequence shown in Fig. 4 could be used to transform from a rolling sphere to a pseudo-jointed robotic arm. With such a morphing system, it would be possible to robotically morph matter into different forms to perform different functions.

VI. Discussion

This letter presents a class of sculpture-inspired robots with the ability to shape-shift on-the-fly, which will enable adaptability in environments with uncertain or variable conditions. The salient criteria of this class of morphable robots are: (1) The robotic skin driving the morphing ability must be well-matched to the material properties of the sculptable body (i.e., the stress generated by the morphing skin exceeds the stiffness of the clay); (2) Any robotic skin operating on a shape-changing body must have distributed actuation and be highly flexible/stretchable to maintain functionality across a wide range of body shapes; (3) The robotic skins must be able to function even while layered on top of each other for the robot to access each of the corresponding behaviors (e.g., shape-change and locomotion).

The primary aim of this work is to present the idea of using passive clay as the body of a robot, and applying robotic function at the surface to sculpt the body into arbitrary shapes. As a first step towards this vision, we demonstrated morphing via motor-driven spooling of cables wrapped around sculptable material (i.e., "clay"). We characterized various types of clay-like materials to understand their mechanical response to applied compressive strain and found that unconfined compression tests are only useful for qualitative comparisons between materials of similar granular structure. Rather, *in situ* force-displacement tests yield more accurate robot characterizations and can be used to select appropriate body materials and robotic skin actuators for this class of robots.

The robotic skins presented in this letter utilize inherently stretchable substrates. By attaching the skins with pre-strain, the skins maintain contact with the clay body, distributing stress across the surface of the clay over a range of body shapes. Additionally, layering the two skins we showed in this letter does not restrict the independent skin functions, and in some ways enhances them. In the obstacle avoidance example shown in Fig. 10, though the locomotion skin is wrapped around the clay underneath the morphing skin, the stretchability of the morphing skin's Spandex can accommodate inflation of the locomotion skin's bladders. Similarly, the locomotion skin's elastomer is resilient to the compression applied by the morphing skin and is able to stretch to accommodate the larger diameter at the ends of the dumbbell.

Furthermore, while we showed only two skins in this work, more skins with other functions could be layered and integrated

into a single, multifunctional robot. However, as the number of skins increases, logistical issues such as cable management and skin interactions must be considered.

While we demonstrated morphing between various radially symmetric shapes, the concept of surface-driven shape-change can extend to asymmetric deformation (*e.g.*, contraction or bending along the length of the clay as shown in Fig. 4B). Returning to our inspiration, we note that sculptors use pinching and smearing motions to create fine features and complex shapes. For a robotic system, incorporating a mechanism to press small bending actuators against the sculptable material would be one possible way to achieve this motion. Other future work includes evaluation of further candidate materials to measure compatibility with both large-scale shape-changes and finer sculpting motions.

VII. Conclusions

Typically, roboticists need to know the functions that a robot is meant to accomplish *a priori*, and this set of functions defines the shape of the robot. In order to accomplish a broader range of tasks or to be able operate in environments with unknown or highly variable conditions, one approach is to allow the robot to adapt its shape.

In this letter, we have presented robotic skins that wrap around sculptable material as a way to create shape-changing robots. Pairing morphing and locomotion behaviors together illustrates the potential of morphing robots that derive versatility from their ability to adapt their shape. The robotic skins were fabricated as stretchable planar substrates with embedded actuation. The morphing skin used cables to squeeze the core material into different shapes, and the locomotion skin utilized sequential inflation of bladders to roll the system. We showed how mechanical characterization of the sculptable material can be used to inform the actuation requirements of the morphing skin. Finally, we demonstrated an application where locomotion was posited as the performance task, and morphing was required to overcome an obstacle.

References

[1] D. Lobo, E. B. Feldman, M. Shah, T. J. Malone, and M. Levin, "Limbform: A functional ontology-based database of limb regeneration experiments," *Bioinformatics*, vol. 30, no. 24, pp. 3598–3600, 2014.

[2] D. Rus and M. T. Tolley, "Design, fabrication and control of soft robots," *Nature*, vol. 521, no. 7553, pp. 467–475, May 2015.

[3] C. Laschi, B. Mazzolai, and M. Cianchetti, "Soft robotics: Technologies and systems pushing the boundaries of robot abilities," *Sci. Robot.*, vol. 1, no. 1, 2016, doi: 10.1126/scirobotics.aah3690..

[4] S. Kim, C. Laschi, and B. Trimmer, "Soft robotics: A bioinspired evolution in robotics," *Trends Biotechnol.*, vol. 31, no. 5, pp. 287–294, May 2013.

[5] M. T. Tolley *et al.*, "A resilient, untethered soft robot," *Soft Robot.*, vol. 1, no. 3, pp. 213–223, Aug. 2014.

[6] R. F. Shepherd *et al.*, "Multigait soft robot," *Proc. Nat. Acad. Sci.*, vol. 108, no. 51, pp. 20 400–20 403, Dec. 2011.

[7] J. Zou, Y. Lin, C. Ji, and H. Yang, "A reconfigurable omnidirectional soft robot based on caterpillar locomotion," *Soft Robot.*, vol. 5, pp. 164–174, Jan. 2018.

[8] S. W. Kwok *et al.*, "Magnetic assembly of soft robots with hard components," *Adv. Functional Mater.*, vol. 24, no. 15, pp. 2180–2187, 2014.

[9] S. A. Morin *et al.*, "Using click-e-bricks to make 3D elastomeric structures," *Adv. Mater.*, vol. 26, no. 34, pp. 5991–5999, Sep. 2014.

[10] M. A. Robertson and J. Paik, "New soft robots really suck: Vacuum-powered systems empower diverse capabilities," *Sci. Robot.*, vol. 2, no. 9, 2017, doi: 10.1126/scirobotics.aan6357.

[11] J. W. Booth *et al.*, "OmniSkins: Robotic skins that turn inanimate objects into multifunctional robots," *Sci. Robot.*, vol. 3, no. 22, Sep. 2018, doi: 10.1126/scirobotics.aat1853.

[12] F. Ilievski, A. D. Mazzeo, R. F. Shepherd, X. Chen, and G. M. Whitesides, "Soft robotics for chemists," *Angewandte Chemie*, vol. 123, no. 8, pp. 1930–1935, Feb. 2011.

[13] V. Wall, R. Deimel, and O. Brock, "Selective stiffening of soft actuators based on jamming," in *Proc. IEEE Int. Conf. Robot. Autom.*, May 2015, pp. 252–257.

[14] F. Daerden and D. Lefeber, "Pneumatic artificial muscles: Actuators for robotics and automation," *Eur. J. Mech. Environmental Eng.*, vol. 47, no. 1, pp. 11–21, 2002.

[15] A. Sprwitz, A. Tuleu, M. Vespignani, M. Ajallooeian, E. Badri, and A. J. Ijspeert, "Towards dynamic trot gait locomotion: Design, control, and experiments with Cheetah-cub, a compliant quadruped robot," *Int. J. Robot. Res.*, vol. 32, no. 8, pp. 932–950, 2013.

[16] S. Kriegman, N. Cheney, and J. Bongard, "How morphological development can guide evolution," *Sci. Rep.*, vol. 8, no. 1, Sep. 2018, Art. no. 13934.

[17] E. Steltz, A. Mozeika, N. Rodenberg, E. Brown, and H. M. Jaeger, "JSEL: Jamming skin enabled locomotion," in *Proc. IEEE/RSJ Int. Conf. Intell. Robots Syst.*, Oct. 2009, pp. 5672–5677.

[18] J. W. Booth, J. C. Case, E. L. White, D. S. Shah, and R. Kramer-Bottiglio, "An addressable pneumatic regulator for distributed control of soft robots," in *Proc. IEEE Int. Conf. Soft Robot.,* Apr. 2018, pp. 25–30.

[19] S.-S. Park, "Effect of fiber reinforcement and distribution on unconfined compressive strength of fiber-reinforced cemented sand," *Geotextiles Geomembranes*, vol. 27, no. 2, pp. 162–166, Apr. 2009.

[20] S. R. Kaniraj and V. G. Havanagi, "Compressive strength of cement stabilized fly ash-soil mixtures," *Cement Concrete Res.*, vol. 29, no. 5, pp. 673–677, May 1999.